HAIFA: A modular, fiber-optic coupled, spectroscopic diagnostic for plasmas

Alan T. Ramsey

Princeton Plasma Physics Laboratory, Princeton University, Princeton, New Jersey 08544

Stephen L. Turner

Science Applications International Corporation, Oak Ridge, Tennessee 37830

(Received 10 December 1986; accepted for publication 23 March 1987)

HAIFA is a modular, multichannel, fiber-optically coupled spectroscopy diagnostic for tokamak plasmas. It operates in the visible, measuring H_α radiation, the visible continuum from thermal bremsstrahlung, and selected impurity lines. HAIFA is characterized by high modularity and flexibility, good radiation resistance, high noise immunity, and low cost. Details of design, construction, and calibration are given. The analysis of visible bremsstrahlung radiation measurements to deduce the effective ionic charge in a plasma is discussed.

INTRODUCTION

A modular, low-cost spectroscopy system using interference filters and fiber-optic coupling has been in use on the Princeton Plasma Physics Laboratory's tokamak fusion test reactor (TFTR) since 1983. This is not the first system of its type; it grew out of the diagnostic that Fonck and co-workers installed on the Princeton divertor experiment (PDX) tokamak in 1980.[1] At MIT, a system independently developed by Foord, Marmar, and Terry to view the visible bremsstrahlung emission from the Alcator C tokamak shares some features with the Princeton system.[2] Morgan and co-workers have installed a fiber-optic system on the joint European torus (JET), which they have described briefly.[3] The Princeton system has not been described previously in any detail, and the TFTR version differs from the MIT and JET systems in several important respects.

HAIFA is a system that collects light from the plasma using simple telescopes, transports it about 50 m in optical fibers to a shielded environment, collimates the light and passes it through one or more interference filters to select emission lines or other spectral regions of interest, detects the light with photomultipliers or photodiodes, amplifies and filters the signals, and then digitizes and stores them for analysis. The system is characterized by high optical throughput (hence, high sensitivity), immunity to both electrical noise and ionizing radiation, reliability and ease of operation, flexibility, and low cost.

In Sec. I, we shall outline the system performance goals and how they are reflected in the final design. In Sec. II, the system components and construction details are described in detail. Section III sketches the uses of HAIFA on TFTR, and includes a discussion of our absolute wavelength and intensity calibration technique. In Sec. IV, we present some brief comments on data analysis, and show sample data from TFTR as examples of how HAIFA is used.

I. DESIGN GOALS AND THEIR IMPLEMENTATION

In this section we shall describe our design goals and how they are met in the system we built. In order of importance, the goals were high system sensitivity and selectivity, good rejection of external noise, high flexibility in application, and low cost.

Although the acronym for the system derives from H-Alpha Interference Filter Array (HAIFA), the most important use is the measurement of the visible bremsstrahlung radiation emitted by tokamak plasmas. This diagnostic tool, first described by Kadota *et al.*,[4] yields valuable information about the purity of the plasma. At the normal operating parameters of TFTR and most other tokamaks, the bremsstrahlung radiation is quite weak; the surface brightness is typically 10^{10} photons/(s cm^2 Å sr). By comparison, radiation in a moderately bright line like H_α (6563 Å) has 10^2–10^3 times more photons, and an impurity ion like O VI can radiate 10^5–10^6 times more photons in a single line. The system for the bremsstrahlung, then, not only must be sensitive, it also must have good rejection of other lines.

A standard figure of merit in the discussion of optical system performance is the throughput, or étendue. The units are (area) × (solid angle). If the plasma is viewed by an optical system which collects all the light from an area A emitted into a solid angle Ω, this product $A\Omega$ multiplied by the surface brightness gives the maximum signal [in photons/(s Å)] that one can collect. To avoid signal loss downstream in the optical system, one must not reduce the geometrical étendue. The HAIFA collection optics are an $f/2$ lens imaging the plasma onto a single fiber with a 600-μm-diam core. This yields an étendue of 5×10^{-4} cm^2 sr. By comparison, the ordinary grating spectrometer we use in the visible ($R = 0.6$ m, $f/7$ grating) has an étendue only slightly less when the slits are opened to give the 10-Å passband used in HAIFA. Moreover, the efficiency of a grating with a favorable blaze angle is about the same as the transmission of an interference filter, and the same detector can be used for either.

We chose to use filters rather than a conventional spectrometer for several reasons. First, the cost of even a simple spectrometer is enormously greater than the cost of an interference filter, and we were designing a system with an ultimate size of more than 40 channels. Second, to achieve a

 0034-6748/87/071211-10$01.30

ratio of 10^6 : 1 in off-resonance rejection requires a double monochromator; scattered light from a single grating instrument would be too great. Third, the coupling of optical fibers to the entrance slit requires some effort, since the fibers have numerical apertures corresponding approximately to an $f/2$ light cone, and are round, while spectrometers are typically $f/5$–$f/8$ with rectangular slits. Crossed cylindrical lens can do the matching job reasonably well, but increase the number of elements and the alignment problems unnecessarily.

The choice of detectors was straightforward. To maintain the modularity, individual detectors were required, and photomultipliers have no competition for gain × bandwidth with low noise. For the H_α channels, we had 10^2–10^3 times more signal than in the visible bremsstrahlung passband, and used photodiodes. Noise in our photodiodes is ten times higher than our photomultipliers at the same operating parameters, but the H_α signal was large enough to make that irrelevant. The cost is lower, the lifetime longer, and most importantly for operational considerations, the gain is more stable. In more than a year of operation after initial turn-on, the measured change in photodiode sensitivity was 15%. By comparison, a new photomultiplier tube may drift 10%–20% in four weeks of operation, although in most well burned-in tubes the change is less, with 5% being typical.

Noise in a tokamak environment is severe. A typical plasma in TFTR is a pulse of 2.5-MA circulating current confined by a pulsed magnetic field of 5 T. A runaway tail of the electron velocity distribution can create a shower of gamma rays of 20-MeV energy when it strikes the vacuum vessel, and even in relatively cool plasmas ($T_{ion} \leqslant 5$ keV) large numbers (10^{15}/s) of thermonuclear neutrons are produced when high-energy neutral beams of deuterium are injected into the deuterium plasma to heat it. Finally, there is substantial mechanical/thermal stress and vibration. By carrying the optical signal in fibers to a remote location, sensitive components are protected. The only elements at the tokamak for a single channel are a simple SiO_2 lens viewing the plasma through a SiO_2 window, a SiO_2 optical fiber, and an aluminum mount. High-purity fused silica is the best optical material for resistance to ionizing radiation,[5] and the telescopes and fibers easily tolerate the 150 °C temperatures the vessel reaches during bakeout. The optical fibers are run to a data-acquisition room some 40–60 m away from the viewing ports, which are located at eight locations distributed around the torus. The attenuation of signals through this length of fiber is less than the coupling losses at each end, and no electrical noise can propagate. The data-acquisition room is well shielded from radiation and vibration. Distance and careful electrical isolation reduce electrical noise to nondetectable levels.

A plasma diagnostic should be flexible. The configuration of the plasma is frequently changed, and as the physics interest changes as the program develops, different regions of the plasma become important. We designed our filter housing so that the interference filters are easy to change and adjust. We can change viewing locations on the machine with ease; all we must do is move a small (32-mm-diam, 150-mm-long) telescope and re-aim it. By directing a He–Ne laser back up the fiber, the telescopes can be both focused and aimed. In the detector rack, any fiber can be connected to any filter housing by loosening one screw. Either type of detector attaches to any filter housing. Not only is this flexibility vital for changing the operating mode, but it makes repair very simple: a failed unit either can be swapped out with one of a small variety of spares, or replaced by a part from a less important channel in an emergency.

Finally, the design was done with an eye to high commonality. The collecting telescopes and the prefilter collimators are identical, for example. Screws for assembly are of two sizes only (2-56 and 6-32). As much as possible, all parts require a minimum of machining from standard stock sizes, so that only a finishing cut (or none) is required for some dimensions.

II. DETAILS OF DESIGN AND CONSTRUCTION

Figure 1 is a simplified block diagram of the system. We shall discuss the components of the system in sequence, starting at the tokamak end.

A. Telescopes and collimators

The telescopes are mounted on the machine in two ways. The single telescopes are held in a mount which clamps around the edge of a 2.75-in. Conflat™ flange (we machined dimples in the flange rim to accept the clamp screws). A 25-mm-diam quartz window is mounted in the flange. The mounted windows are from Huntington, model VPQ-150. This window will tolerate temperatures to 200 °C. We have repeatedly cycled them to 150 °C with no failures. One window failed, however, due to mechanical problems. The construction of the window leaves the seal exposed, and great care must be used in handling and installation. The

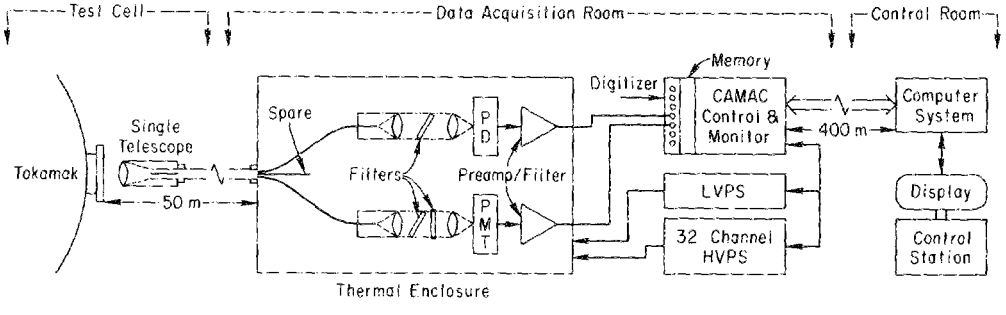

FIG. 1. The HAIFA system block diagram, showing one telescope and fiber-optic cable. Most telescopes have three fibers connecting them to the data-acquistion room.

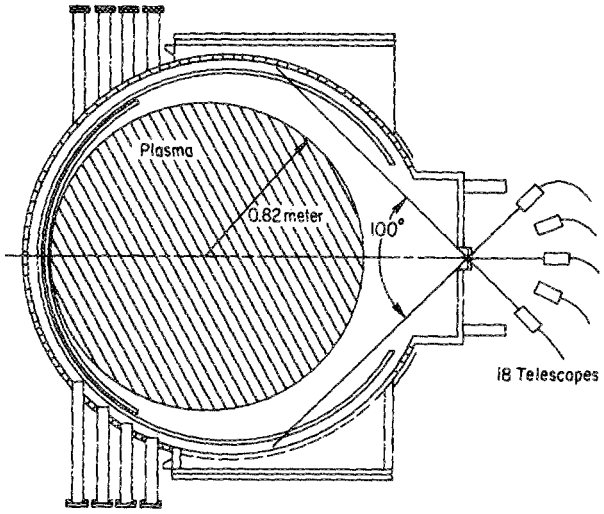

FIG. 2. Poloidal array of telescopes. There are 18 telescopes in the array, each with three fibers at the image plane. The telescopes are steerable about two axes for adjustment.

single telescope mount allows the viewing angle to pivot $\pm 3°$ about the window normal.

The telescopes in the poloidal array are mounted in steerable blocks on an arch whose center is a 4-in. sapphire window (from Ceramaseal) in a 6.5-in. Conflat™ flange. The array contains 18 telescopes, and covers a poloidal angle of $-50°$ to $+50°$, measured from the horizontal. The viewing lines span all of even the largest plasmas. (See Fig. 2.)

The telescope consists of a lens, a lens holder and body, and a focus slide. (See Fig. 3.) The lenses are high-purity fused silica (Melles-Girot 01-LPQ-001), with a focal length of 50 mm and a diameter of 25 mm. They are simple, and plano-convex since we use them near infinity focus. The cylindrical telescope body has a registration key which fits into the telescope holder for reproducible orientation. The focus slide holds the fiber, which is terminated in a metal ferrule.

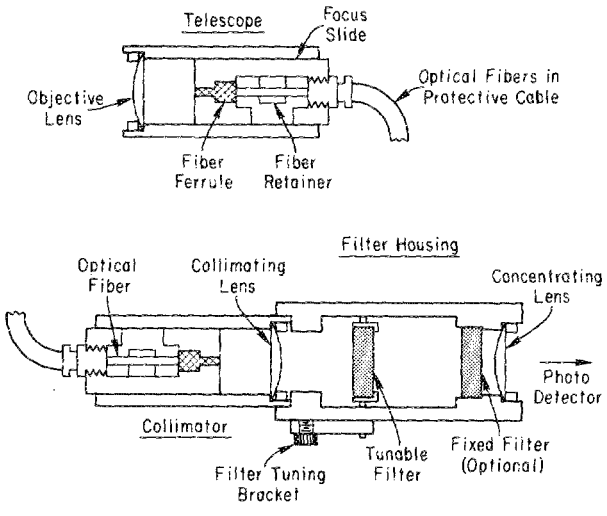

FIG. 3. Telescope/receiver, interference filter in its housing, and detector. The telescope and collimator are identical. The filter housing shows a filter in the rotating holder. The shoulder to the right holds a second filter normal to the collimated rays when this is required.

The ferrule is clamped concentrically inside the slide, and the fiber itself is further clamped to the slide for strain relief of the ferrule. The slider is keyed to the inside of the telescope body. The telescopes are 150 mm long and 32 mm in diameter. Normally the slide is set so that the end of the fiber is imaged at the other side of the vacuum vessel (about 2.5 m) for tightly collimated light collection. A fitting at the end of the focus slide clamps an opaque 0.25-in.-diam plastic protective tubing in the telescope.

In the data-acquisition room, the fibers in use are connected to collimators, which produce a parallel ray bundle to pass through the interference filters. The collimators are identical to the telescopes with one exception: the lenses are glass. There is no radiation and no elevated temperature to contend with, and the cost of a glass lens is less than a tenth that of a high-purity SiO_2 lens.

B. Fiber-optic cables

The fiber used is high-purity fused silica with a 600-μm-diam core, surrounded by a silicon polymer cladding and a Tefzel™ protective outer jacket. The total diameter is about 1 mm. The fiber is Fibropsil QSF-600A, manufactured by Quartz et Silice, France, and marketed in the United States by Quartz Products Corporation of Plainfield, NJ. Our selection, made several years ago, was based on tests of the then available fibers conducted by the Naval Research Laboratory on the effects of ionizing radiation on optical transmission. The Fibropsil fibers showed excellent radiation resistance in the visible. A review by Sigel summarizes research in the radiation resistance of optical fibers.[5] Most of the telescopes have three fibers in a tight circular array at the focus of the lens. While the use of three fibers increases the cost slightly over a single fiber of equivalent cross section, it has two marked advantages. First, it gives redundant light paths. Of the 24 cables we have made so far, one was damaged in the installation and one was broken by operations nearby. In both cases only one of the three fibers was damaged. Second, each telescope can be connected to as many as three separate filter/detector assemblies simply by fitting the fiber ferrules into the collimator slides. The use of beam splitters requires more parts, critical alignment, and lacks the flexibility of detector choice and location which individual fibers offer.

The three-fiber cables are prepared as follows: Because the fiber cladding (which forms the total internal reflection interface) is a soft polymer which cannot be glued or clamped, it and the outer protective jacket must be stripped off before a fiber can be terminated. The stripped fiber is cleaned with acetone and reclad by dipping into a solvent-based compound (Epotek 394) which dries to the proper optical index. This results in a hard cladding which can be glued. A standard ferrule (Amphenol 906, although others would be equivalent here) is drilled out to 1.40 mm (a number 54 drill) to accept the fibers in a triangular array. An optical epoxy designed for the purpose (Epotek 302) is used to glue the fibers into the ferrule. When the epoxy is cured, we grind the ends of the fibers flush with the ferrule and polish them. Since this is a light-gathering system and not an imaging device, the polishing is very simple. Three ferrules

can be mounted in a jig and polished at one time on our 8-in. laps. A coarse diamond lap (200 μm) is used for the rough grinding. The surface is then polished on aluminum oxide laps of 30-, 12-, 3-, and, finally, 1-μm grit. Examination with a microscope shows no visible scratches. The entire process takes about 10 min.

To test the quality of the bond, we performed a pull test by attaching weights to one fiber of a three-fiber ferrule. At an applied load of 5 kg to the 1-mm fiber, the attachment of the weight to the fiber jacket failed repeatedly, but the ferrule joint held. Examination with a microscope while the joint was under load showed no signs of deformation.

The attachment of ferrules to single fibers at the other end of the cables is much simpler. Mechanically bonding ferrules (Radiall F 706054000) used with a fiber cleaver (Radiall Optall F 780014000) give good terminations in about 2 min. These devices are designed specifically for the QSF fibers. The strength of the attachment is high (although this end of the fiber is under very little stress), and a mistake in the process costs little in time or money.

In making up the cables, it is easiest to thread the optic fibers through 20-m sections of protective tubing at a time. One can push the fibers through this length. Adjacent sections of tubing are connected with ordinary tubing connectors to reach the total length of the run. There are no joints or splices in the fibers themselves. In the data-acquisition room, the protective cable is connected by fittings to the relay rack which holds the detectors. Inside the rack, the fibers have a large strain relief loop before attaching to the collimators.

Our experience shows that the protective tubing should have a distinctive color if it is to be routed along with other more robust cables. The black Eastman Polyflow™ tubing we started with looks exactly like coaxial cable; however, it is much more susceptible to damage by kinking, which usually breaks the contained fiber.

C. Filters

The interference filters are 25 mm in diameter, of three-cavity construction, and blocked to 10 000 Å. We obtained them from Barr Associates of Westford, MA. Interference filters have three main types of central frequency shift. As they age, they drift blue. As they are heated, they drift red. As the angle of incidence of the light to be filtered varies from the normal, they tune blue. We designed our system so that the filter mounts would tilt, allowing us to tune the filters. The thermal drift is 0.1–0.3 Å/K, depending on details of the filter construction, according to Corion Corporation of Holliston, MA. One H_α filter we tested had a temperature coefficient of 0.19 Å/K. We have found very little age drift in several years of operation (perhaps an Ångstrom for an H_α filter), but this depends critically on the filters' environment. The angular shift is about 0.4 Å/(degree^2) for angles near the normal. We keep our filters in a temperature-stabilized cabinet at 33 °C (see below), higher than room temperature ever rises. We ordered them 5 Å red of the desired center wavelength, which gives about 10 Å of slack for manufacturing tolerance. All of our filters have been well within that tolerance. The filters for the visible bremsstrahlung (at 5235 Å) and for the H_α measurements (6563 Å for H, 6561 Å for D, 6560 Å for T) were ordered with 10-Å passbands. The added width from the diverging collimated beam (due to the finite source size of 600 μm) is negligible on this scale.

A simple ring with diametric exterior pins serves as a tiltable filter mount; see Fig. 3. A lever on the outside of the filter housing attaches to one of the pins and tilts and clamps the filter at the correct angle.

The filter detector housings also have a mounting collar for a second filter. We felt that obtaining more than 1000 : 1 rejection of light outside the passband was beyond the current state of the art even for a three-cavity filter. Therefore, we used a second broadband (45 Å) filter, mounted in series with the first for compound rejection. The two filters are at an angle of 10° to each other to avoid spurious cavity effects. The 45-Å passband of the broad filter allows a relatively high transmission ($\approx$60%) without including any bright lines. It may be possible, however, to obtain comparable performance with a single filter.[6]

Following the tilted fiber and the (optional) normally mounted filter, the light falls on a field lens (glass) which concentrates the light onto the detector. The spot size on the photomultipliers (see below) is smaller than the photocathode size so that we are sure the view is not vignetted. The extended image avoids two dangers of a smaller spot size: accelerated wear of the photocathode and sensitivity to small shifts in the optical system. (Such sensitivity could be due to local variations in photocathode response which are averaged out with a large illuminated area.) The same approach is used with the smaller photodiode photocathodes.

D. Thermal housing

A relay rack in the data-acquisition room is the terminus for the fiber cables. The protective jackets are secured to a panel of the rack with bulkhead tubing feedthroughs, and the rack contains a large ($2\times0.5\times0.5$ m) insulated box. The temperature is controlled by a simple proportional controller (Cole-Parmer Versatherm 2156 with a YSI-621 sensor) driving four 60-W lightbulbs as heating elements. Two are at the top of the cabinet, two are at the bottom, and a fan circulates the air. The temperature is measured (an Omega Digicator with a 411A readout) and fed into a CAMAC analog-to-digital converter for remote monitoring. The box is maintained at about 33 °C; the drift is less than 1 °C, which does not move any of our filter passband edges over a line.

The thermal enclosure also contains the detectors and preamplifiers. This is a matter of convenience, but has the advantage of stabilizing the dc offset in the preamps. It does not affect the intrinsic system noise.

E. Detectors

The wavelength of the visible bremsstrahlung region is centered at 5235 Å. However, we wanted to look at impurity lines, too, so we needed extended blue response in our photomultipliers. We chose the RCA 4837. This tube is from the 1P28 family; a nine-stage, side-viewing photomultiplier with a fused silica window and an Sb–Cs photocathode. However,

perhaps its most important characteristic was its very low dark current (1.5×10^{-11} A at 100 A/lm) which was important for our sometimes very low signals. This tube is no longer made. We are evaluating the Hamamatsu R212, which appears to be an equivalent tube. The photomultipliers are housed in Pacific Precision Instruments 315-ORF housings. The bias chain uses only resistors and capacitors. The housing is rf shielded, and the filter housing mounts rigidly to the PMT housing with an O-ring for a light seal. The PMT housing contains a combination magnetic/electrostatic shield.

The photodiode detectors are the EG&G HUV 1000B. This is a blue-enhanced silicon photodiode operated in the zero bias (photovoltaic) mode, and has an integral op-amp, all in a TO5 housing. We operate the op-amp with a 20-MΩ feedback resistor in the current input mode, and use the same $\pm$ 15 V dc power that the preamps (see below) use. The photodiode/amplifier was mounted on a small board in a box that clamps to the filter housing exactly as the PMT housing does. The detector is held concentric with the field lens by a Teflon™ annular ring. Fine adjustment of the detector position relative to the field lens is made by spring-loaded mounting screws which hold the board to the box.

F. High voltage

We use a LeCroy 4032A high-voltage power supply. This is a CAMAC-interfaced 32-channel supply designed to operate photomultipliers and similar low-current devices. The cost is less than the equivalent number of individual supplies. Also the unit has very attractive control, monitor, and alert features. Experience has shown, however, that this trade-off should be examined more carefully. The mean time between failures for the 4032A is less than a year, and all our failures (four on the HAIFA unit, three on another unit at this laboratory) have affected all 32 channels. While the summed failure rate of individual supplies may be greater, a failure in one such unit does not affect other data channels. Also, the modularity and low unit cost of individual supplies mean easier replacement and cheaper spares expenses. Supplies such as the Bertan PMT-10A can be programmed and monitored remotely by CAMAC D/A's and A/D's with no interfacing other than cables. Our experience with supplies of the Bertan type suggests that their MTBF is much longer.

G. Preamplifiers

The requirements for the preamps are not stringent. A gain of 100 V/μA is sufficient to drive the digitizers with the photomultiplier voltages at 650 V, typical. There were several features we wanted, however, that made us design our own preamp.

We use both photodiode/amplifiers and photomultipliers, so we need both voltage and current preamplifiers. Our units have a jumper on the input resistor which is quickly attached or removed to change from one mode to another. The gain, while not changed often is critical for data analysis and should be easy to monitor. There are three gains (100, 10, and 1 V/μA in the current mode; 100, 10, and 1 V/V in the voltage mode) which are switch selected at the preamp and reported through CAMAC. This gain monitoring requires only 2 bits, and the fourth status (chosen to be low–low) indicates no power to the preamp.

Before digitizing an analog signal it must be filtered to avoid aliasing, and we have included an active three-pole filter into our preamp with a roll-off of more than 18 dB/octave above the knee. We usually run the digitizers at 2 kHz, so that the knee is set at 1 kHz, but sometimes we want to examine faster phenomena. To facilitate changes in the filter frequency, the filter components were made accessible. Because these were to be general purpose spectroscopy preamps, we wanted an output stage that could drive long cables if necessary, so a high-current output was included. Finally, since saturation of our signals is possible, saturation should be clearly shown. Therefore, the output is clamped at 5 V, before any of the amplifier stages start to overload. The design is very conservative, and the circuit is well bypassed and shielded. With over 100 unit-years operation, we have had only one failure.

H. Digitizers

The preamps are fed directly into BiRa Systems model 908 CAMAC-based digitizers, strapped for -5 to $+5$-V operation. Although we operate the preamplifiers at nominal zero bias and therefore use only half the digitizer's resolution here, it eases problems of dc offset and drift (the preamps are dc coupled, since the plasma pulse lasts as long as 6 s), and there is sufficient resolution (4000 counts, full scale) for our purposes. The digitized output is stored in local memory and read back after the pulse is over.

I. ac power supply

All ac power for the system is routed through four solid-state ac relays. We designed a switching box which allows either local or remote (via CAMAC) control of these relays, and returns an on/off status of each circuit. Our access to the hardware is quite limited during normal operations. These circuits allow us the capability of being able to turn off, say, the high-voltage power supply or the rack heater if there is a malfunction in either of these units. Both of these events have occurred, and we view this control as necessary. The unit also gives us a direct and independent measurement that the ac power is really on.

III. CALIBRATION AND NOISE

After the fiber-optic cables are in place, telescope/collimators are attached to each end and focused. We used a He–Ne laser injected through the lens onto the fiber as a light source. The telescope/collimator's focus slide at the other end was adjusted to focus the image of the fiber on some suitably distant surface. The slide then was locked down.

Before the collimators are installed in the filter housings, the filters are tuned. We used a monochromator as a tunable source for this purpose. A fiber mounted at the exit slit is terminated at the other end with a collimator, which is inserted into the filter housing. After the absolute wavelength was checked (moving the monochromator the 800 m from our lab to the data-acquisition room typically jars the wavelength setting several Ångstroms) the monochromator

is tuned to the desired wavelength. The filter mount is tilted until the passband is centered on the monochromator line by measuring the preamp output. It is important that the filter housing be at the operating temperature (33 °C in our case) during this procedure so that temperature dependence does not shift the tuning. In more critical cases, we measure the filter passband by scanning the monochromator and recording the preamp output. This must be done in the case of the H_α–D_α filters. Absolute intensity measurements of these lines are made to measure particle influx to the plasma, and we must be sure that the filter totally covers both lines. For the bremsstrahlung filters it is not necessary, since they sample the continuum.

When the filters are aligned and the complete system is connected, from telescope through digitizer, an *in situ* system absolute intensity calibration is done. Our absolute source is a tungsten ribbon lamp, the General Electric 30A/T24/13, available from Eppley Laboratory, Newport, RI. The supplier will calibrate the lamp; however, we had our lamps calibrated by the National Bureau of Standards.[7] The lamp with its assorted support apparatus cannot be set up at the tokamak, so a transfer standard is used. It consists of a dedicated telescope, 5 m of fiber, collimator, filter, detector, high-voltage power supply, and preamp. The transfer standard is first calibrated in the lab using the ribbon lamp. A laser illuminates the fiber with light at the collimator end, and the end of the fiber at the telescope is imaged (using an auxiliary lens) onto the center of the standard lamp's filament. If the image of the fiber is smaller than the filament width, we are assured that the lamp is filling the optics of the calibration channel. The lamp is turned on and set (using a precision shunt resistor and a potentiometer) to a current at which the NBS calibration was done.

NBS calibrates a lamp with a photoelectric pyrometer. The lamp's current is adjusted until its output, measured by the pyrometer, matches that of a secondary blackbody at the temperature desired. (The secondary blackbody is calibrated against the primary radiometric source, gold at its freezing point.) This brightness matching is done at a specified wavelength, usually 6550 Å. The surface brightness of the filament is given by the blackbody equation

$$B = \epsilon(\lambda, T) 2c\lambda^{-4} (e^{-hc/(kT\lambda)} - 1)^{-1} . \quad (1)$$

The units are photons/(s wavelength area sr), and all the symbols have their usual meanings.

The temperature in this equation is the true surface temperature; the calibration, which has not taken the emissivity of the tungsten filament into account, gives the filament's brightness temperature (as seen through the lamp's envelope window). To use the lamp at wavelengths other than the calibration wavelength, we need to find the surface temperature at the calibration current, and then use the appropriate value of $\epsilon(\lambda, T)$ for the wavelength of interest. Between 3000 and 6000 Å, and between 1600 and 2800 K, $\epsilon(\lambda, T)$ varies between 0.44 and 0.48. Tables of the emissivity can be found in several places.[8]

In the visible, and for temperatures in the 2000–2500 K range, the relation between the surface temperature and the brightness temperature is closely approximated by

$$T_s = T_B / \{1 + T_B \times (\lambda k / ch) \times \ln[\epsilon(\lambda, T) t_\lambda]\} , \quad (2)$$

where t_λ is the transmission of the lamp envelope quartz window. The value of t_λ can be taken as 0.92, constant over the visible wavelength range. Equation (2) is an implicit solution for T_s; the value for $\epsilon(\lambda, T)$ is that corresponding to T_s, not T_B. However, the error in determining T_s will be only about 1.5 K when using the value of $\epsilon(\lambda, T)$ for T_B, which gives an error in the brightness of less than 1%.

Now that we know the true surface brightness of the filament at our calibration current, we can measure the response of the transfer standard to the light. One practical problem is that the calibration lamp is much brighter than the visible bremsstrahlung; in our case the brightness of the lamp at the lowest calibration current is 1.2×10^{14} photons/(s Å cm^2 sr), and the plasma's brightness is typically only 1×10^{10}. This difficulty can be dealt with using calibrated neutral density filters in front of the transfer channel telescope when it is being calibrated. We were able to use the known gain ratios of the preamps, and exploit the very wide linear range of photomultipliers. Care must be taken in this approach, however, to avoid saturating the tube. A chopping wheel in front of the standard lamp eliminates stray light and dc offset problems. An oscilloscope or a digital voltmeter reading peak to peak are satisfactory ways to measure the preamp output.

After the transfer standard is calibrated in the lab using filters similar to the ones used in the HAIFA channels on the tokamak, the *in situ* system calibration can be done. The transfer standard telescope is mounted beside the telescope(s) of the channel(s) to be calibrated at the tokamak. We use a quartz–halogen projection bulb to illuminate a target in front of the telescopes. A chopper wheel modulates the signal. The specifications of the light source do not matter (although the source must be incandescent) because the transfer standard views it over the same wavelength range as do the channels to be calibrated. Nor does the width of the filters in the transfer standard matter; the calibration automatically accounts for that. The center wavelength has a slight effect, however. Near 5230 Å, which is commonly used for measurements of the visible bremsstrahlung because of the absence of lines, a difference of 10 Å between bandpass centers of the transfer standard and the channels to be calibrated gives an error of about 2% at a lamp temperature of 2200 K. At 2700 K, the error has fallen to 1%. At the D_α wavelength (6563 Å), the errors are half this size.

The kind of target viewed by the transfer standard and the channel(s) to be calibrated is not important as long as it does not show specular reflections. We have used ordinary bond typing paper successfully. For calibrating the array, which views $\pm$ 50° from the normal, we sandblasted an aluminum sheet and painted it with flat white optical paint (3M™ Nextel 101–10A). We measured the diffuse reflectivity as a function of viewing angle, and found a slow, smooth falloff that was down to 90% of the normal value at 50°. We could see no specular component for this target.

Next let us consider the transmission of the windows and lenses in the system. We inferred the surface tempera-

TABLE I. The cumulative noise in the detector chain for a typical visible bremsstrahlung channel, in terms of the equivalent brightness signal.

Cumulative rms noise photons/(s Å sr cm^2)			
Digitizer	+ Preamp	+ PMT (HV on)	+ Plasma Signal = 1×10^{10}
9.0×10^6	1.0×10^7	5.5×10^7	3.3×10^8

ture of the absolute calibration lamp filament by correcting for the window transmission. When we calibrated the transfer standard, we did it through the SiO_2 lamp window and the SiO_2 lens used to fill the telescope optics. This loss of about 15% is compensated for by the two elements through which the telescopes view the plasma, i.e., the vacuum window and the protective shutter inside the vacuum vessel, both of which are SiO_2. Measurements of both windows and shutters verify that the two-surface loss of clean SiO_2 is indeed 8%. The protective shutter does not stay clean, however, nor would the window if the shutter were not there. The purpose of the shutter is not so much to keep the window clean as to allow us to measure the transmission of the dirty element. This we do by remotely swinging the shutter out of the field of view for one of a sequence of identical plasma shots and comparing signal strengths. During the last run of TFTR, the array shutter transparency fell from 0.92 to 0.32 over a period of only four months. The changes in transmission are episodic rather than gradual, and usually can be traced to a specific plasma discharge which disrupted violently.

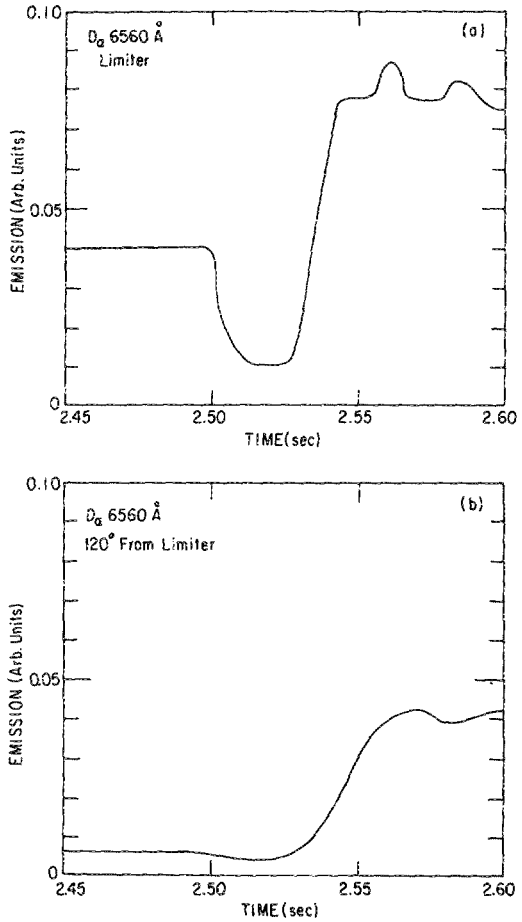

FIG. 4. D_α emission from two toroidal locations, showing a free expansion of the plasma from 2.50 s until hard limiting on the inner wall begins at 2.55 s.

Table I shows the noise from the different parts of the system and from a plasma of moderate brightness. These data are all digitally rebinned for an equivalent sample time of 20 ms. This was the usual filtering prior to display and analysis. The unrebinned data of the system noise alone, taken at the standard 0.5-ms sample time, show a noise level about 20% higher than a bandwidth dependence of ($\partial\,\mathrm{Hz}^{-1/2}$) would predict when compared with the 20-ms noise, reflecting the preamplifier roll off above 1 kHz.

An estimate of the photon-counting statistics noise, based on reasonable values of losses and efficiencies in the various parts of the system, indicates that for a moderate brightness of $B = 1\times10^{10}$ photons/(s Å cm^2 sr), an rms counting noise figure of 1×10^8 photons/(s Å cm^2 sr), or 1%, would be expected. The 3% value observed arises from other sources in the plasma itself. Table I shows that the contribution to the total noise from system noise is not significant.

In Sec. I, we said that the detector noise in the photodiode channels is a factor of 10 higher than in the photomultiplier channels. However, the signal integrated over the H_α or D_α lines (depending on the plasma working gas) is typically 100–1000 times stronger, so that the photodiodes are quite satisfactory for this purpose.

IV. DATA AND ANALYSIS

HAIFA is used on TFTR primarily to study H_α radiation from the plasma edge and bremsstrahlung radiation from the entire plasma volume. In this section, we show data illustrating these uses and briefly discuss the analysis techniques.

Five channels monitor the radiation as the neutral fuel atoms are excited and ionized at the edge of the plasma. This H_α and D_α radiation (at 6563 and 6561 Å, respectively) comes from the very edge of the plasma where the electron temperature is only 10's of eV and the electron density is in the range of 5×10^{12} cm^{-3}. When the detectors are absolutely calibrated, the integrated total brightness of this radiation can be turned into a particle influx into the plasma and, when combined with information about the plasma size and density, can yield values for particle confinement times.[3] This calculation requires some modeling and is not done routinely. The raw data, however, can furnish other useful information. For example, Fig. 4 shows the D_α intensity during a free expansion discharge. Initially the plasma is constrained by a limiter on the outer edge of the plasma. Most of the deuterium recycling into the plasma does so at or near the plasmas contact point on the limiter, so that the channel which is viewing 120° away sees little or no radiation. At 2.5 s, the plasma is moved magnetically inward, the signal at the limiter drops, and the plasma begins to expand at about 7 mm/ms until it is in contact with the inner wall of the vessel,

at which time one sees the signal increase at both locations.[9]

The second major use of HAIFA is to monitor the radiation from bremsstrahlung at 5235 Å. Observations with our visible spectrograph show that there are no lines within the filter passband. That being so, the volume emissivity observed is, for a single ionic target species,

$$\epsilon = 1.89\times 10^{-28}\, n_e n_i Z_i^2\, g_{\rm ff}(i, T_e) T_e^{-1/2} \lambda^{-2} \times \exp(-12\,400/T_e\lambda)\,, \quad (3)$$

where ϵ is the volume emissivity in W/(cm^3 Å), n_e and n_i are the electron and ion densities, respectively, in number/cm^3, Z_i is the effective charge state of the impurity species (i), $g_{\rm ff}(i,T_e)$ is the Maxwellian-averaged free–free Gaunt factor for this charge state and electron temperature, T_e is the average electron temperature in electron volts, and λ is the wavelength in Ångstroms.[4,10] In the visible, the exponential term is so nearly equal to 1 that it is dropped. The question of what is the effective ionization state, Z_i, for a heavy impurity ion is a complex one,[11,12] which we shall ignore because our impurities are dominated by C and O, which are completely stripped in the vast bulk of the radiating plasma. Thus when Eq. (3) is summed over impurities, we take Z_i to be the atomic number of the impurity and $g_{\rm ff}$ is taken outside the summation, even though it has a dependence on Z_i and T_e. This allows us to write

$$\epsilon = 1.89\times 10^{-28}\, n_e^2 \lambda^{-2} T_e^{-1/2} g_{\rm ff} Z_{\rm eff}\,, \quad (4)$$

where we have used the common definition of Z effective

$$Z_{\rm eff} = \sum (n_i/n_e) Z_i^2\,. \quad (5)$$

It is this convenient form that allows us to calculate some kind of average $Z_{\rm eff}$ from the emissivity and use it in the analysis of plasma behavior. The question arises: What error is made by taking an effective $g_{\rm ff}$ outside the summation over target ions? We have evaluated this error for several TFTR scenarios. Taking various impurity mixes, and using the exact value of $g_{\rm ff}$ from Ref. 10, the value of $g_{\rm ff}(i,T_e)$ was compared with an effective value for $g_{\rm ff}$ (as parametrized below), $\langle g_{\rm ff}\rangle$. The results are shown in Table II.

The first two cases are typical of moderately clean TFTR plasmas, where the dominant impurity is carbon. The error is less than 1%. The second two cases are pathological but possible discharges where the dominant impurity is Ni (from Inconel protective plates inside the vacuum vessel).

TABLE II. The results of using an effective value for the free–free Gaunt factor and ignoring the detailed dependence on charge state and temperature, compared to the exact value calculated from Ref. 10 for several representative cases from TFTR plasmas.

Impurity mix				$\langle g_{\rm ff}\rangle$
n_i/n_e(C)	n_i/n_e(Ni)	$n_i/n_e(Z=7)$	$Z_{\rm eff}$	$g_{\rm ff}(i,T_e)$
3.3%	0.0%	0.0%	2.0	1.00
10.0%	0.0%	0.0%	4.0	1.00
0.0%	0.4%	0.0%	4.0	0.92
0.0%	0.7%	0.0%	6.0	0.91
0.0%	0.1%	8.0%	5.4	0.98

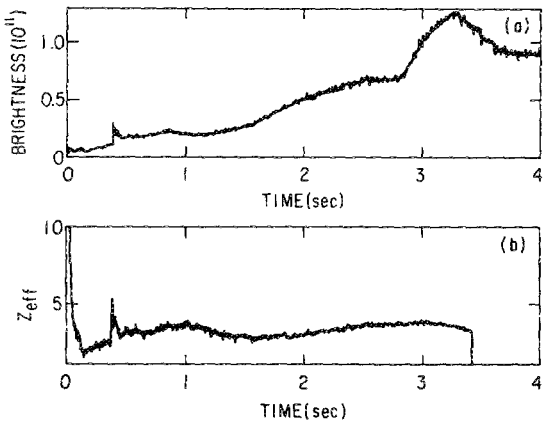

FIG. 5. Measured visible bremsstrahlung brightness and the calculated Z effective from a plasma discharge on TFTR. The units of brightness are photons/(s cm^2 Å sr). At 2.8 s, a heating beam of neutral deuterium was injected into the plasma, driving the density and temperature up substantially. The Z effective falls slightly during this injection due to dilution of the plasma by heating beam ions.

In these cases the error could be nearly 10%; moreover, the question of what the effective charge state of the Ni ions is further confuses the relationship between impurity concentration and $Z_{\rm eff}$. The last case is more usual for a dirty mixed impurity discharge, where a mixture of carbon and oxygen is joined by 0.1% Ni. The error here is only 2%, which is too small to be important even for systematic studies, and is well within the intensity calibration uncertainty.

The variation of the Gaunt factor with ion and temperature cannot be ignored. Between 100 and 5000 eV, and for plasma ions with atomic numbers between 1 and 28 (typical values for modern tokamaks), $g_{\rm ff}$ varies from 1.8 to 4.7. Fortunately, the variation is slow and smooth, and if one parametrizes the values in Ref. 10 in a double power law, the Z and T_e dependencies can be combined with those in Eq. (4). For the range of impurities and temperatures of TFTR, we find a good approximation to be

$$g_{\rm ff} = 3.77 Z_{\rm eff}^{-0.0579} T_e^{0.147}\,. \quad (6)$$

Our experience on TFTR is that there is little or no radial variation in $Z_{\rm eff}$ for most types of plasma (see below). That being so, the emissivity in Eq. (4) can be integrated across a diameter of the plasma with $Z_{\rm eff}$ outside the integral, giving a relation between the surface brightness of the plasma and the $Z_{\rm eff}$. This brightness is what a telescope looking through the middle of the plasma sees, ignoring for now reflections from the walls of the vacuum vessel (but see below). The integral over the temperature and density profiles either can be done exactly using, for example, Thomson scattering data, or the profiles can be modeled with only a peak temperature and the line-integrated density as inputs. The profiles themselves often do not change much, and their radial integrals change even less as the plasma conditions change.

Figure 5 shows the results of such a simple calculation, which is done automatically after each shot and is presented within seconds. The brightness time history is from a central channel of the visible bremsstrahlung array. The calculated $Z_{\rm eff}$ time history uses this brightness, a temperature profile

from our electron cyclotron emission radiometer,[13] and the line-integrated density from our 1-mm interferometer.[14] The density profile is modeled; it is approximately parabolic. The high value of $Z_{\rm eff}$ at the beginning of the discharge is an artifact. Neither the brightness nor the temperature is reliable this close to the plasma start up. The burst at 0.4 s is from a sudden influx of carbon; at this time the plasma swept across a cracked carbon tile in TFTR's movable limiter. The plasma reached equilibrium at about 2.5 s when both the plasma current and density had stabilized. This particular plasma had a current of 2.2 MA, a central density of 6.2×10^{19} m^{-3}, and a central electron temperature of 4.0 keV. Its major radius was 2.56 m, its minor radius was 0.82 m, and the toroidal field at the center of the plasma was 4.7 T. These conditions were typical of large plasmas on TFTR at the end of the 1984–85 run period. At 2.8 s, 5.3 MW of high-energy neutral deuterium atoms were injected into the plasma. As a result, the density increased substantially, and the visible bremsstrahlung brightness doubled. However, the impurity fraction of the plasma, as indicated by the $Z_{\rm eff}$, did not increase; in fact, beginning at about 3 s there was a slight decrease caused by dilution. The $Z_{\rm eff}$ calculation was terminated at 3.4 s, the last time for which T_e data were available immediately after the shot. A more detailed analysis is done for selected shots off line. This latter analysis uses full profile information and smoothed and adjusted data. The results of the two calculations seldom differ by as much as 10%.

The third main use of the HAIFA system is to gather poloidal profile data from the 18-channel visible bremsstrahlung array. When these chordal data are inverted to yield a volume emissivity profile, the results can be combined with temperature and density profiles to determine the radial dependence of $Z_{\rm eff}$. Figure 6 shows data from the poloidal array for a discharge with nearly the same parameters as the one shown in Fig. 5, except that the injected power is higher. The upper figure is the chordal data, folded about the horizontal midplane of the plasma. The nonzero chordal intensity outside the plasma (at 50°) is due to reflections from the stainless-steel vacuum vessel walls. The measured brightness outside the plasma is about 10% of the central chord brightness during ohmic discharges for a large variety of plasma parameters and geometries. This will distort the Abel inversion process, and as a correction, all channels are assumed to see the same reflected light, and 10% of the central channel is subtracted from each. (After the inner wall of TFTR was covered with carbon protective tiles, the reflections disappeared.) The neutral beam injection which began at about 2.8 s deposited 5.6 MW in the plasma, heating the ions to 4.3 keV in the plasma center. The electron temperature rises slightly during neutral injection, which would cause the emission at 5253 Å to decrease. However, the major effect is a sharp increase in emission caused by the density increase. The inverted data are shown in Fig. 6(b). We do our inversions by least-squares fitting to orthogonal polynomials in

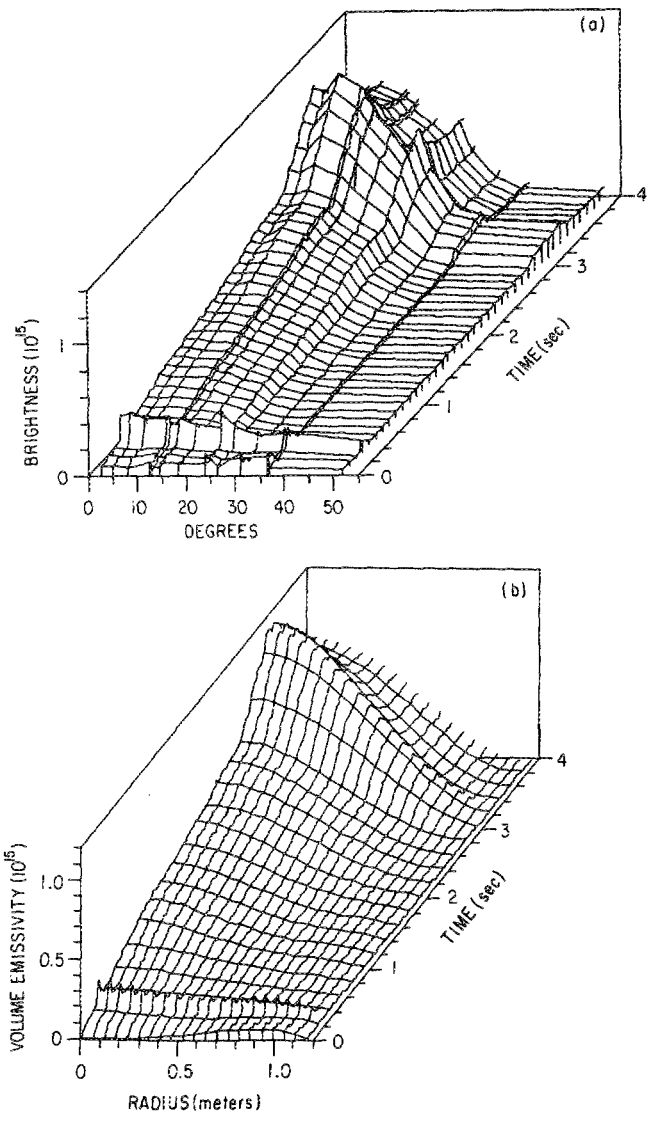

FIG. 6. (a) The chordal data from the bremsstrahlung array for a shot with neutral atom heating beam injection at 2.8 s. The event at 100 ms is the growing plasma sweeping across a broken carbon tile on the plasma limiter. The edge signal is mostly reflected light; some real emission does occur outside the limiter, however. (b) The Abel inversion of the data in (a). This is a reconstruction using polynomials up to degree 4; higher orders give a better picture of edge variation (where it exists) but are too sensitive to noise to give reliable central reconstructions.

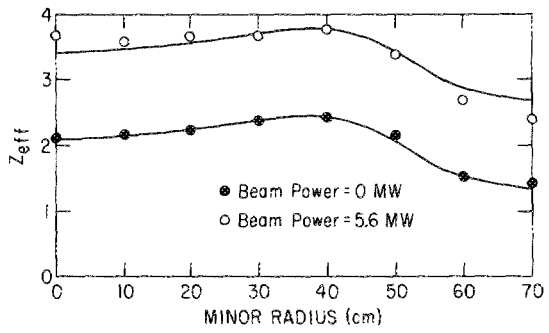

FIG. 7. The Z-effective radial profiles from inverted chordal data. The upper curve is a profile from the emissivity of the shot in Fig. 6. The lower curve shows the Z profile of a shot without neutral beam injection, but with the same size, density, and current. For both shots, $I_p = 2.2$ MA, $B_T = 4.7$ T, $n_e = 4.5\times10^{19}$ m^{-3}, the major radius is 2.5 m, and the minor radius is 0.82 m. To aid comparison, the two smooth curves are identical, and are merely displaced from one another.

emission or physical space, not in chordal or integrated space. Thus we can change the polynomial degree and have a clear physical picture of what we are doing. In the inversion in Fig. 6(b) we have used polynomials up to 4th degree; higher orders tend to generate noise in the center for this shot.

We remarked earlier that our Z_{eff} radial profiles are essentially flat. In Fig. 7, we have taken temperature and density profiles, and extracted $Z_{\text{eff}}(r)$ from the inversion shown in Fig. 6 at the end of neutral beam injection. From the center to 50 cm, the value is flat to $\pm$ 6%. A pronounced drop at 60 and 70 cm may be real (an accumulation of impurities in the center of a plasma has been seen before) or could be an artifact of the Thomson scattering density measurement, which is rather hard to make at the outer edge of the plasma where the density is low. The 36% fall in the calculated value of Z_{eff} could stem from an 18% systematic error in $n_e(r)$ at these points, which is possible.

The more general question of errors in Abel inverted profiles is difficult to answer; details of each system must be considered. What is true in all cases is that systematic errors in the outer chords have a cumulative effect on the inferred central brightness. One check we have used is to make sure that the central $Z_{\text{eff}}(r)$ agrees with the value derived from the central chord integrated with the measured $T_e(r)$ and $n_e(r)$ profiles. For the inverted Z_{eff} profile shown in Fig. 7, the central chord value agreed well with the central value of the profile. [Note that because of the $n_e^2(r)$ term in Eq. (4), the central chord determination is strongly centrally weighted.] We have done sensitivity tests with our inversion process, and believe that for plasmas such as the one measured in Fig. 6, the error in the central brightness is less than 20%.

ACKNOWLEDGMENTS

C. Mayo of Science Applications International Corp. was responsible for much of the design and testing of the preamplifier, as well as the detail design of the optical detector assembly. J. Bartolick was a valuable source of advice during design and fabrication, and assisted in the installation, alignment, and calibration of the system on TFTR. E. Thomas painstakingly assembled the myriad parts of the 36 channels of our initial set, and saw them safely installed and connected in the thermally controlled rack. P. Sichta was responsible for the CAMAC interface of HAIFA to the TFTR on-line computer system. Control and analysis software was written by T. Terpstra, W. Davis, W. Journey, V. Locasale, N. Schechtman, and M. Diesso. This work was supported by the United States Department of Energy under Contract DE-AC02-76-CHO-3073.

[1] A. T. Ramsey, R. J. Fonck, and R. V. Yelle, Bull. Am. Phys. Soc. **25**, 938 (1980).
[2] M. E. Foord, E. S. Marmar, and J. L. Terry, Rev. Sci. Instrum. **53**, 1407 (1982).
[3] P. D. Morgan, K. H. Behringer, P. G. Carolan, M. J. Forrest, N. J. Peacock, and M. F. Stamp, Rev. Sci. Instrum. **56**, 862 (1985).
[4] K. Kadota, M. Otsuka, and J. Fujita, Nucl. Fusion **20**, 209 (1980).
[5] G. H. Sigel, Jr., Proc. IEEE **68**, 1236 (1980).
[6] A. Smaikowitz, Barr Associates, Westford, MA (private communication).
[7] A description of the calibration method and a brief bibliography can be found in the NBS publication NBSIR 84-2875, the NBS Physical Measurement Services Status Report for 1984. The contact for calibration work at NBS is R. Wilkinson, Radiometric Physics Division, National Bureau of Standards, Washington, DC 20899; telephone (301) 921-3613.
[8] The data in any recent edition of the *Handbook of Chemistry and Physics*, published by the Chemical Rubber Company, Cleveland, are adequate for most uses. For a detailed study, see J. C. De Vos, Physica **20**, 690 (1954). For data extending below 2500 Å, see J. L. Buckley, Appl. Opt. **10**, 1114 (1971).
[9] G. Tait *et al.*, *Plasma Physics and Controlled Nuclear Fusion Research 1984*, Vol. I (International Atomic Energy Agency, Vienna, 1985), p. 141.
[10] W. J. Karzas and R. Latter, Astrophys. J. (Suppl.) **6**, 167 (1961). See also Ref. 11.
[11] T. Kato and H. Narumi, Plasma Physics Institute, Nagoya University, Report IPPJ-AM-6, 1978.
[12] V. P. Zhdanov, Sov. J. Plasma Phys. **4**, 71 (1978).
[13] G. Taylor, P. Efthimion, M. McCarthy, V. Arunasalam, R. Bitzer, J. Bryer, R. Cutler, E. Fredd, M. A. Goldman, and D. Kaufman, Rev. Sci. Instrum. **55**, 1739 (1984).
[14] P. C. Efthimion, G. Taylor, W. Ernst, M. Goldman, M. McCarthy, H. Anderson, and N. C. Luhmann, Rev. Sci. Instrum. **56**, 908 (1985).